Future Changes in Precipitation Extremes in East Asia and Their Uncertainty Based on Large Ensemble Simulations with a High-Resolution AGCM

Hirokazu Endo[1], Akio Kitoh[2], Ryo Mizuta[1], and Masayoshi Ishii[1]
[1]*Meteorological Research Institute, Tsukuba, Japan*
[2]*University of Tsukuba, Tsukuba, Japan*

Abstract

Future changes in precipitation extremes in East Asia are investigated using large ensemble simulations of about 100 members by a 60-km mesh atmospheric general circulation model (AGCM) for the present climate and 4 K warmer climates, employing six different sea surface temperature (SST) anomaly patterns projected by state-of-the-art climate models. The high-resolution AGCM demonstrates good performance for reproducing precipitation extremes such as annual maximum 1-day precipitation total (Rx1d). Under the warmer climates, Rx1d are robustly projected to increase throughout East Asia. However, there is large range of their quantitative estimates, arising from internal variability and uncertainty in future SST patterns. Over land regions such as inland China, internal variability is the major source of the uncertainty in climatological-mean Rx1d change. However, over oceanic regions including Japan, Korea and coastal China, uncertainty in the SST patterns contributes greatly to the uncertainty in Rx1d through modulation of tropical cyclone activity, suggesting large regional variations in the relative importance of the two sources of uncertainty.

(**Citation**: Endo, H., A. Kitoh, R. Mizuta, and M. Ishii, 2017: Future changes in precipitation extremes in East Asia and their uncertainty based on large ensemble simulations with a high-resolution AGCM. *SOLA*, **13**, 7−12, doi:10.2151/sola.2017-002.)

1. Introduction

East Asia is a water-rich area and is often affected by water-related disasters due to extreme rainfall events, monsoons, typhoons, etc. Quantitative regional climate projections of precipitation extremes and their uncertainty under global warming are of high demand especially for impact studies and adaptation planning. The Intergovernmental Panel on Climate Change (IPCC) Fifth Assessment Report (AR5) stated that heavy precipitation is very likely to increase at the end of the 21st century in the East Asian monsoon region, and projected a 20% increase on the median estimate of the summer season maximum 5-day precipitation total in the East Asian monsoon region, under the Representative Concentration Pathways 8.5 (RCP8.5) scenario, based on atmosphere-ocean coupled general circulation models (AOGCMs) in the Coupled Model Intercomparison Project phase 5 (CMIP5) (Christensen et al. 2013). However, these AOGCMs have limited applicability to studies with much finer time/spatial scales because of their coarse horizontal resolution, typically of the order of 200km. In addition, AOGCMs suffer from systematic biases associated with sea surface temperature (SST) bias in their present-day simulations, reducing confidence in their regional climate projections (Kitoh et al. 2016).

High-resolution atmospheric general circulation models (AGCMs) with grid sizes of 20 km and 60 km have been developed at Meteorological Research Institute (MRI) to overcome these problems (Mizuta et al. 2006, 2012). The models have been extensively applied to climate change studies and in particular to extreme phenomena, including tropical cyclones (TCs) (Oouchi et al. 2006; Murakami et al. 2012a, 2012b; Sugi et al. 2016), precipitation extremes (Kamiguchi et al. 2006; Endo et al. 2012; Kitoh and Endo 2016a, 2016b), and Baiu–Meiyu precipitation in East Asia (Kusunoki et al. 2006, 2011; Kitoh and Kusunoki 2008). The results have shown that the high-resolution AGCMs perform well in reproducing climatology as well as extremes, and they are superior to lower-resolution versions. Other high-resolution modeling activities unanimously demonstrate the capability of simulating TCs and precipitation extremes (Wehner et al. 2014; Roberts et al. 2015; Kodama et al. 2015). We note that in our experimental settings, present-day SST are taken from an observation, and future SSTs are created by adding the future changes projected by AOGCMs to the observed present-day values, thereby minimizing the effects of SST biases involved in AOGCMs (Kitoh et al. 2016).

Quantifying uncertainty in future climate projections is necessary for impact studies and adaptation planning. On the global scale, major sources of uncertainty come from differences in emission scenarios and climate model formulations (Hawkins and Sutton 2011), which are adequately considered in the CMIP5 experiment framework. On the other hand, internal variability also introduces substantial uncertainty into projections of regional climate and climate extremes (Xie et al. 2015). To adequately estimate this, large ensemble simulations with different atmospheric states have been conducted (Deser et al. 2014; Kay et al. 2015).

Recently, large ensemble simulations, called "Database for Policy Decision-Making for Future Climate Change (d4PDF)", have been performed using a 60-km mesh MRI-AGCM for the present and future climates, employing six different SST anomaly patterns projected by AOGCMs, with a total integration time of over 5000 years for the respective climates (Mizuta et al. 2017). This large ensemble simulation has much larger members and higher horizontal resolution than that of the earlier studies above mentioned; so that it enables us to thoroughly investigate future changes in regional climate and climate extremes, as well as their uncertainty. Using this dataset, our study examines future changes in precipitation extremes in East Asia and discusses their uncertainty by distinguishing the inter-member spread generated by internal variability from that due to differences in future SST patterns. The effect of TCs on the uncertainty is also investigated.

2. Model experiment and validation data

2.1 Model

We used a 60-km mesh MRI-AGCM version 3.2 (MRI-AGCM3.2) (Mizuta et al. 2012), identical to the MRI-AGCM3.2H included in the CMIP5 archive. The 60-km mesh version uses triangular truncation at wave number 319 (T_L319) in the horizontal, with a 640 × 320 grid. There are 64 layers in the vertical with the top at 0.01 hPa. A new mass-flux type scheme (Yoshimura et al. 2015) for cumulus parameterization is incorporated. The 60-km version of MRI-AGCM3.2 realistically simulates climatological fields such as precipitation and moisture flux on the global scale (not shown), with features quite similar to those in the 20-km version (Mizuta et al. 2012).

Corresponding author: Hirokazu Endo, Meteorological Research Institute, 1-1 Nagamine, Tsukuba, Ibaraki 305-0052, Japan. E-mail: hendo@mri-jma.go.jp.

2.2 Experiment design

The present climate for the period 1951 to 2010 is simulated with 100 members, in which the observed inter-annually varying monthly-mean SST and sea-ice concentration (COBE-SST2) (Hirahara et al. 2014) are used as the lower boundary conditions. In addition to the use of different atmospheric initial conditions, small perturbations in SST (δSSTs), varying in space and time, are added to COBE-SST2 for the ensemble simulations. We note that the typical magnitude of δSST for the monthly scale is below 0.2 K (0.2 to 0.4 K) over the western tropical Pacific (East Asia).

For the future climate, a 60-year integration with 90 members is conducted, in which the global-mean surface air temperature (SAT) is 4.1 K (3.6 K) warmer than the pre-Industrial level (present climate (1951−2010)), corresponding to conditions around the 2090s under the RCP8.5 scenario. The future SST data were created by adding CMIP5 AOGCM-projected SST anomalies (ΔSSTs), as a function of longitude, latitude and month, to the observed SST after removal of the long-term trend component. Therefore, the amplitude of warming is kept constant throughout the integration. To properly cover a wide range of uncertainty in the CMIP5 projections, six different ΔSSTs (CCSM4, GFDL-CM3, HadGEM2-AO, MIROC5, MPI-ESM-MR, and MRI-CGCM3) are selected based on cluster analysis using tropical ΔSST spatial patterns (Fig. S1). Note that the ΔSSTs were scaled to obtain a global-mean SAT 4 K warmer than the pre-Industrial level. For each of the six ΔSSTs, 15-member ensemble experiments are conducted using different atmospheric initial conditions and different δSSTs (i.e., 90 members in total). See Mizuta et al. (2017) for details of the experiment design.

2.3 Validation data

To validate precipitation, we used Tropical Rainfall Measuring Mission (TRMM)-3B42 version 6 (Huffman et al. 2007). The TRMM data with 0.25 degree horizontal resolution were first spatially averaged over model grid boxes with T_L319 resolution for comparison with model output. For the atmospheric data, we used the Japanese 55-year Reanalysis (JRA-55) (Kobayashi et al. 2015) with T_L319 resolution. For the observed TC tracks, we used International Best Track Archive for Climate Stewardship (IBTrACS) v03r06 (Knapp et al. 2010).

2.4 Precipitation indices

We used four precipitation indices: summer (May to September) total precipitation (Psum), annual maximum 1-day precipitation total (Rx1d), annual maximum 3-day precipitation total (Rx3d), and annual maximum 10-day precipitation total (Rx10d).

3. Present-day simulations

In East Asia, precipitation extremes such as Rx1d appear mainly during the summer season (May to September) (Fig. S2). Therefore, climatological mean fields in the summer season are first shown. Figures 1a and 1b show Psum for TRMM observation and the simulation, respectively. The model realistically reproduces the rain-band extending from southeastern China to

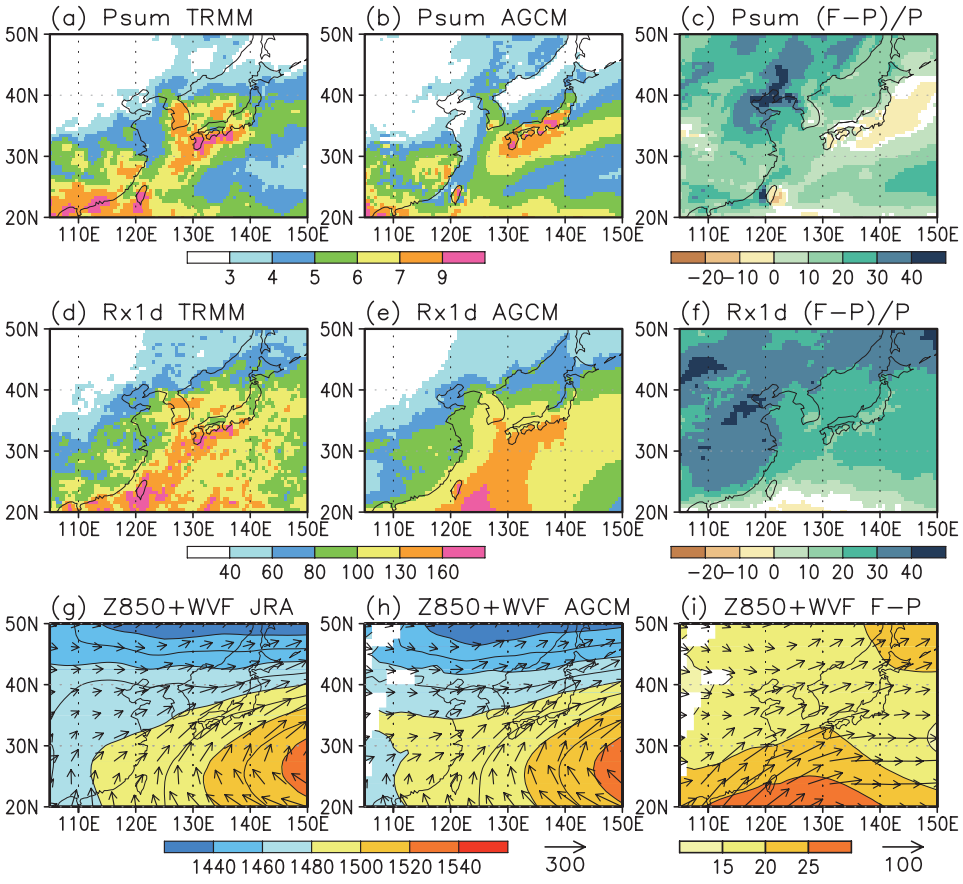

Fig. 1. (left column) Observed climatology, (middle column) simulated present-day climatology, and (right column) projected future changes: (top row) total summer precipitation (Psum; mm day^{-1}), (middle row) annual maximum 1-day precipitation total (Rx1d; mm), and (bottom row) summer average 850 hPa height (shading and contour; m) and vertically integrated moisture flux (vector; kg m^{-1} s^{-1}). Observations are from TRMM-3B42 for (a) and (d) and JRA-55 for (g). The present-day climatology is averages for 1998−2010. The future changes are the percentage change ((F–P)/P*100) between the present climate (P: 1951−2010) and the future climate (F: 60 years in 3.6 K warmer climates) for (c) and (f) as well as the differences (F–P) for (i). All the model data are shown by ensemble averages. Areas with white color in (c) and (f) denote that changes are not statistically significant at the 5% level, while areas with white color in (h) and (i) denote that data is unavailable due to underground. Note that TRMM data were averaged over model grid boxes with TL319 resolution before calculating the precipitation indices.

southern Japan, the so-called Baiu–Meiyu rain-band that characterizes the East Asian summer monsoon, although the model underestimates the rainfall in the western and northern parts of the rain-band.

Figures 1d and 1e show Rx1d. In the observation the area with values exceeding 100 mm covers most of the northwestern Pacific and surrounding regions, and its maximum magnitude exceeds 130 mm from Taiwan through the East China Sea to southern Japan and Korea. Such observed features are very well reproduced by the model, but with a slight eastward displacement of the peak. For Rx3d and Rx10d, although the patterns are realistically simulated, the magnitudes are underestimated in the western and northern components (Figs. S3a, S3b, S3d, and S3e).

Figures 1g and 1h show 850 hPa height (z850) and vertically integrated moisture flux. The simulated moisture flux field is in good agreement with the observed features, with large southerly and southwesterly fluxes along the periphery of the northwestern Pacific subtropical high (NWPSH). However, the area with maximum moisture flux in the model is slightly displaced eastward with respect to the observation, consistent with weaker westward expansion of the NWPSH. This bias seems to be associated with underestimation of Psum in eastern China and eastward displacement of the peak of Rx1d.

4. Future changes and their uncertainty

Figure 1c shows future changes in Psum, indicating increases over most of East Asia and decreases in parts of southern Japan and surrounding areas. Projections of precipitation extremes (Rx1d, Rx3d, and Rx10d) show their increasing throughout East Asia, with larger magnitude than that of Psum (Figs. 1f, S3c, and S3f). In particular, the increase of Rx1d exceeds 30% over eastern China and northern Japan. The area-averaged changes in East Asia (105°E−150°E, 20°N−50°N) for Psum and Rx1d scaled by local SAT change are 3.2%/K and 5.4%/K, respectively. Compared with single member or small ensemble simulations (not shown), the changes projected by large ensemble are smoother and their statistical confidence levels are higher, enabling us to extract the signal rather than the noise. Figure 1i shows that moisture transport from the northwestern Pacific and the South China Sea toward East Asia will be enhanced, due to increased moisture in the atmosphere and intensification of the NWPSH, consistent with some previous studies (Seo et al. 2013; Kusunoki and Mizuta 2013).

Here, we investigate the future change in Rx1d and its uncertainty in more detail. Figure 2a shows ensemble-mean changes in the climatological mean Rx1d ($\Delta\hat{\mu}$), while Fig. 2b shows the total spread among all members for the change in the climatological-mean Rx1d ($\hat{\sigma}_{tot}$). It is found that $\Delta\hat{\mu}$ is much larger than $\hat{\sigma}_{tot}$ throughout East Asia, indicating the robustness of the increases in Rx1d. However, there is large range of about 10% in the total spread ($\hat{\sigma}_{tot}$).

Using a statistical method applied by Rowell et al. (1995) and Sugi et al. (1997), the total variance ($\hat{\sigma}^2_{tot}$) is decomposed into a component due to the difference in ΔSST patterns ($\hat{\sigma}^2_{\Delta SST}$) and a component due to the internal variability seen in the ensemble with different atmospheric initial conditions and δSSTs ($\hat{\sigma}^2_{int}$). See Text S1 in supplementary material for the detailed calculation. Note that the term $\hat{\sigma}^2_{int}$ is not only due to purely atmospheric internal variability but due to the effect of δSST, however, the latter effect could be negligible for our argument because the amplitude of δSST varies in time so that δSST hardly affects the climatological mean Rx1d.

Figures 2c and 2d show the spatial distributions of $\hat{\sigma}_{\Delta SST}$ and $\hat{\sigma}_{int}$, respectively, and Fig. 2e shows the ratio of $\hat{\sigma}_{\Delta SST}$ to $\hat{\sigma}_{int}$. We find that $\hat{\sigma}_{\Delta SST}$ is much smaller than $\hat{\sigma}_{int}$ in land regions such as inland China, whereas $\hat{\sigma}_{\Delta SST}$ is comparable to $\hat{\sigma}_{int}$ in oceanic regions including Japan, Korea, and coastal China, suggesting large regional variations in the relative importance of the two sources of uncertainty.

To gain a better understanding of the regional differences, we defined two domains: domain A (25°N−32.5°N, 105°E−120°E) corresponding to the Meiyu region and domain B (30°N−37.5°N, 125°E−140°E) corresponding to the Baiu region, and compared area averages of $\Delta\hat{\mu}$, $\hat{\sigma}_{tot}$, $\hat{\sigma}_{\Delta SST}$, and $\hat{\sigma}_{int}$ for the precipitation indices (Fig. 3). For changes in the ensemble mean ($\Delta\hat{\mu}$), the indices of heavy precipitation (Rx10d, Rx3d, and Rx1d) are projected to increase more greatly than Psum; and their magnitudes are larger as the time scale is shorter, with larger increases for domain A than

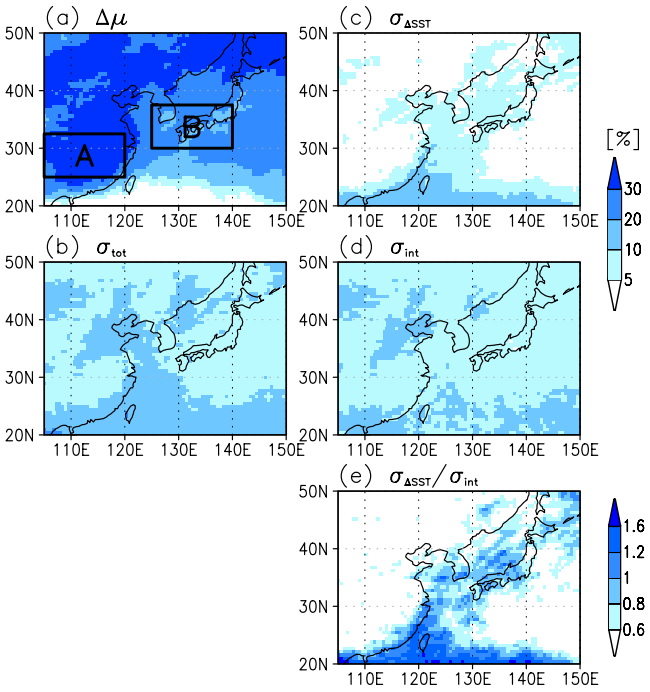

Fig. 2. Future percentage changes in climatological mean Rx1d and their uncertainty. (a) Ensemble average ($\Delta\hat{\mu}$; %), (b) ensemble spread among all members ($\hat{\sigma}_{tot}$; %), (c) ensemble spread coming from difference in future SST patterns ($\hat{\sigma}_{\Delta SST}$; %), (d) ensemble spread coming from internal variability ($\hat{\sigma}_{int}$; %), and (e) the ratio of $\hat{\sigma}_{\Delta SST}$ to $\hat{\sigma}_{int}$.

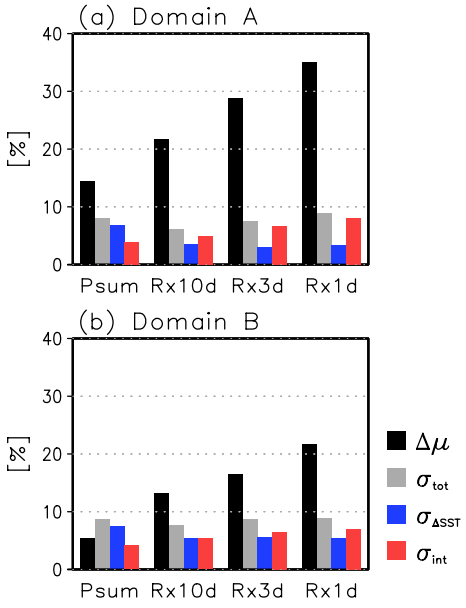

Fig. 3. Area-average values of $\Delta\hat{\mu}$, $\hat{\sigma}_{tot}$, $\hat{\sigma}_{\Delta SST}$, and $\hat{\sigma}_{int}$ for the precipitation indices over (a) the domain A (25°N−32.5°N, 105°E−120°E) and (b) the domain B (30°N−37.5°N, 125°E−140°E) as indicated in Fig. 2a. Note that all the values are first calculated on the original grid and then averaged over the domains.

for domain B. The projected increases are robust for almost all indices because of much larger increase in $\Delta\hat{\mu}$ than the magnitude of $\hat{\sigma}_{tot}$. The exception is Psum in domain B, where $\Delta\hat{\mu}$ is smaller than $\hat{\sigma}_{tot}$, suggesting the existence of some uncertainty in the sign of Psum change in the Baiu region.

The relative importance of the SST pattern ($\hat{\sigma}_{\Delta SST}$) and internal variability ($\hat{\sigma}_{int}$) in terms of the total uncertainty ($\hat{\sigma}_{tot}$) for the heavy precipitation indices is different in the two regions: internal variability is the major source of uncertainty in domain A, especially for Rx1d, while the SST pattern largely contributes to the total uncertainty in domain B (i.e., magnitudes of $\hat{\sigma}_{\Delta SST}$ and $\hat{\sigma}_{int}$ are similar). For Psum, in contrast, $\hat{\sigma}_{\Delta SST}$ is much larger than $\hat{\sigma}_{int}$ in both regions, suggesting the tropical SST distributions force larger-scale circulation changes and may be important for Psum changes (Mizuta et al. 2014).

5. Precipitation extremes associated with tropical cyclones

Heavy precipitation events in East Asia are often associated with TCs. Here, following Kitoh and Endo (2016b), TC-associated precipitation is defined as that within a 500 km radius of TC centers; and then Rx1d associated with TCs (Rx1d-TC) and Rx1d not associated with TCs (Rx1d-nTC) are defined.

Figures 4a and 4b indicate the model generally reproduces well the spatial distribution of the climatological-mean Rx1d-TC, with greater than 100 mm in lower latitudes and exceeding 80% in the ratio of Rx1d-TC to Rx1d over the east off Taiwan (not shown), although with some underestimation around Japan. The negative bias seems to be associated with less frequency of TC occurrence simulated by the model (Figs. S4a and S4b), which is somewhat improved in the 20-km version of MRI-AGCM (Kitoh and Endo 2016b). The model also reproduces well the spatial distribution of Rx1d-nTC, with some underestimation (overestimation) in the western (eastern) part of the Baiu–Meiyu rain-band (Figs. 4d and 4e).

As for future changes, Rx1d-TC is projected to decrease in lower latitudes, but increase in higher latitudes (Fig. 4c), for which the former could be associated with less activity of TCs in the western North Pacific (Fig. S4c), as pointed out by Kitoh and Endo (2016b). On the other hand, Rx1d-nTC is projected to increase throughout East Asia with the rate of about 20% to 40% (Fig. 4f), which largely contributes to increased Rx1d in East Asia (Fig. 1f).

Figure 5a presents the ratio of the spread of the ΔSST pattern uncertainty to that of internal variability (i.e., $\hat{\sigma}_{\Delta SST}/\hat{\sigma}_{int}$) for future changes in the climatological-mean Rx1d-TC. Larger values are found over oceanic regions, including the western North Pacific, the East China Sea, the Sea of Japan, and surrounding areas. The spatial distributions of Rx1d and Rx1d-TC resemble each other (Figs. 2e and 5a). In contrast, the distribution for Rx1d-nTC has a different appearance, with weaker signals (Fig. 5b). These suggest that differences in ΔSST patterns modulate TC activity, resulting in large uncertainty in changes in heavy precipitation over oceanic regions.

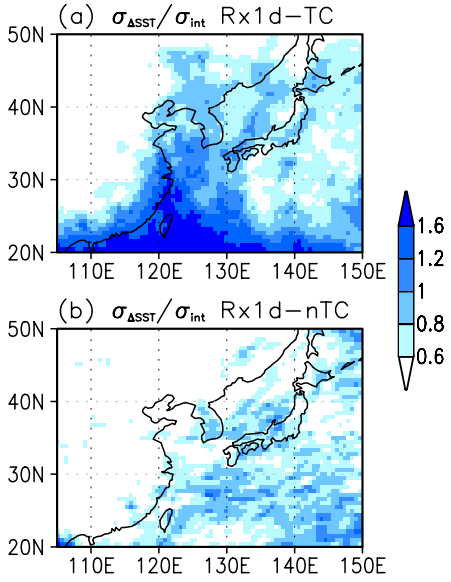

Fig. 5. Same as Fig. 2e except for (a) Rx1d-TC and (b) Rx1d-nTC.

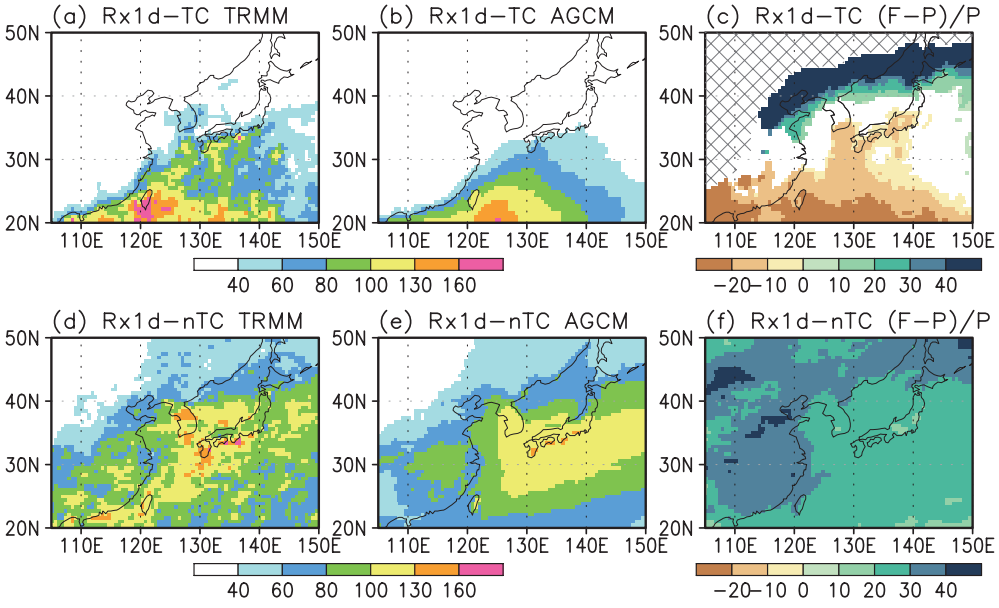

Fig. 4. Same as Figs. 1d, 1e, and 1f except for (a–c) Rx1d associated with tropical cyclones (Rx1d-TC) and (d–f) Rx1d not associated with tropical cyclones (Rx1d-nTC). For (c), area with Rx1d-TC below 1 mm in the present climatology (1951−2010 average) are masked by hatching with grey. The observed TC tracks are from International Best Track Archive for Climate Stewardship (IBTrACS) v03r06 (Knapp et al., 2010). The criteria detecting simulated TC are based on Murakami et al. (2012a).

6. Concluding remarks

This study analysed large ensemble projections under 4 K warmer climates using a high-resolution AGCM, revealing a robust increase in precipitation extremes such as Rx1d throughout East Asia. Over land regions such as inland China the uncertainty in the climatological-mean Rx1d change is derived mainly from internal variability. However, over oceanic regions including Japan, Korea and coastal China, the difference in future SST patterns contributes to the uncertainty through modulation of TC activity. The results indicate there are large regional variations in the relative importance of these two sources of uncertainty. This information would be useful in configuring large ensemble projection using AGCMs with limited computational resources. To appropriately estimate the range of uncertainty, ensemble projection involving different SST patterns within the CMIP5 model spread should be configured over regions where SST pattern differences have importance for the uncertainty.

Our results also show that TCs make a large contribution to Rx1d in the present-day climatology as well as to the uncertainty in its future changes, suggesting realistic representation of TCs in climate models is essential for reliable future projection of precipitation extremes. Therefore, the use of high-resolution climate models is indispensable. Many studies have indicated that in general the total number of TCs will decrease but very intense TCs will increase in a warmer world (Murakami et al. 2012b; Knutson et al. 2015; Kitoh and Endo 2016b; Bacmeister et al. 2016). Such a unique response of TC activity to global warming may affect a future change in the probability distribution function of Rx1d in TC-affected regions. This topic should be investigated in a future work.

Finally, we note that as differences in model structure introduce another source of uncertainty in projections, a multi-model set of large ensemble projections is ultimately desirable. As of now, another set of ensemble projections consisting of a multi-SST and multi-physics with 12 members using the 60-km mesh AGCMs is available (Endo et al. in preparation), thus it would provide helpful information about the uncertainty. It is also noted that there are concerns that non-representation of air–sea interaction within the AGCM may cause too many intense TCs and poleward shift of their distribution (Ogata et al. 2016) and distort the precipitation distribution over the western tropical Pacific (Wang et al. 2005). To solve this issue, our modeling group has been developing an AOGCM with high-resolution atmospheric component, with the aid of flux adjustment to ensure realistic SST field (Ogata et al. 2016).

Acknowledgements

This study was supported by the SOUSEI program and the Data Integration and Analysis System (DIAS), sponsored by the Ministry of Education, Culture, Sports, Science and Technology. The Earth Simulator was used as “Strategic Project with Special Support” of JAMSTEC. Also, the authors thank M. Sugi of MRI and two anonymous reviewers for giving useful comments as well as K. Yoshida of MRI for providing TC tracking data.

Edited by: H.-H. Hsu

Supplement

Supplement 1 contains one text section and four figures.

References

Bacmeister, J. T., K. A. Reed, C. Hannay, P. Lawrence, S. Bates, J. E. Truesdale, N. Rosenbloom, and M. Levy, 2016: Projected changes in tropical cyclone activity under future warming scenarios using a high-resolution climate model. *Climatic Change*, doi:10.1007/s10584-016-1750-x.

Christensen, J. H., and co-authors, 2013: Climate phenomena and their relevance for future regional climate change, in Climate Change 2013: The Physical Science Basis. *Contribution of Working Group I to the Fifth Assessment Report of the Intergovernmental Panel on Climate Change*, T. F. Stocker et al., Eds., Cambridge Univ. Press, Cambridge, and New York, NY.

Deser, C., A. S. Phillips, M. A. Alexander, and B. V. Smoliak, 2014: Projecting North American climate over the next 50 years: Uncertainty due to internal variability. *J. Climate*, **27**, 2271−2296.

Endo, H., A. Kitoh, T. Ose, R. Mizuta, and S. Kusunoki, 2012: Future changes and uncertainties in Asian precipitation simulated by multi-physics and multi-sea surface temperature ensemble experiments with high-resolution Meteorological Research Institute atmospheric general circulation models (MRI-AGCMs). *J. Geophys. Res.*, **117**, D16118, doi:10.1029/2012JD017874.

Hawkins, E., and R. Sutton, 2009: The potential to narrow uncertainty in regional climate predictions. *Bull. Amer. Meteor. Soc.*, **90**, 1095−1107.

Hirahara, S., M. Ishii, and Y. Fukuda, 2014: Centennial-scale sea surface temperature analysis and its uncertainty. *J. Climate*, **27**, 57−75, doi:10.1175/JCLI-D-12-00837.1.

Huffman, G. J., R. F. Adler, D. T. Bolvin, G. Gu, E. J. Nelkin, K. P. Bowman, Y. Hong, E. F. Stocker, and D. B. Wolff, 2007: The TRMM multi-satellite precipitation analysis: Quasi-global, multi-year, combined-sensor precipitation estimates at finer scale. *J. Hydrometeor.*, **8**, 38−55.

Kay, J. E., and co-authors, 2015: The Community Earth System Model (CESM) large ensemble project: A community resource for studying climate change in the presence of internal climate variability. *Bull. Amer. Meteor. Soc.*, **96**, 1333−1349.

Kamiguchi, K., A. Kitoh, T. Uchiyama, R. Mizuta, and A. Noda, 2006: Changes in precipitation-based extremes indices due to global warming projected by a global 20-km-mesh atmospheric model. *SOLA*, **2**, 64−67.

Kitoh, A., and S. Kusunoki, 2008: East Asian summer monsoon simulation by a 20-km mesh AGCM. *Climate Dyn.*, **31**, 389−401.

Kitoh, A., and H. Endo, 2016a: Changes in precipitation extremes projected by a 20-km mesh global atmospheric model. *Weather and Climate Extremes*, **11**, 41−52.

Kitoh, A., and H. Endo, 2016b: Future changes in rainfall extremes associated with El Niño projected by a global 20-km mesh atmospheric model. *SOLA*, **12A**, 1−6.

Kitoh, A., T. Ose, and I. Takayabu, 2016: Dynamical downscaling for climate projection with high-resolution MRI AGCM-RCM. *J. Meteor. Soc. Japan*, **94A**, 1−16.

Knapp, K. R., M. C. Kruk, D. H. Levinson, H. J. Diamond, and C. J. Neumann, 2010: The International Best Track Archive for Climate Stewardship (IBTrACS): Unifying tropical cyclone best track data. *Bull. Amer. Meteor. Soc.*, **91**, 363−376.

Knutson, T. R., J. J. Sirutis, M. Zhao, R. E. Tuleya, M. O. Bender, G. A. Vecchi, G. Villarini, and D. Chavas, 2015: Global projections of intense tropical cyclone activity for the late twenty-first century from dynamical downscaling of CMIP5/RCP4.5 scenarios. *J. Climate*, **28**, 7203−7224, doi:10.1175/JCLI-D-15-0129.1.

Kobayashi, S., and co-authors, 2015: The JRA-55 reanalysis: General specifications and basic characteristics. *J. Meteor. Soc. Japan*, **93**, 5−48, doi:10.2151/jmsj.2015-001.

Kodama, C., Y. Yamada, A. T. Noda, K Kikuchi, Y. Kajikawa, T.

Nasuno, T. Tomita, T. Yamaura, H. G. Takahashi, M. Hara, Y. Kawatani, M. Satoh, and M. Sugi, 2015: A 20-year climatology of a NICAM AMIP-type simulation. *J. Meteor. Soc. Japan*, **93**, 393−424, doi:10.2151/jmsj.2015-024.

Kusunoki, S., J. Yoshimura, H. Yoshimura, A. Noda, K. Oouchi, and R. Mizuta, 2006: Change of Baiu rain band in global warming projection by an atmospheric general circulation model with a 20-km grid size. *J. Meteor. Soc. Japan*, **84**, 581−611.

Kusunoki, S., R. Mizuta, and M. Matsueda, 2011: Future changes in the East Asian rain band projected by global atmospheric models with 20-km and 60-km grid size. *Climate Dyn.*, **37**, 2481−2493.

Kusunoki, S., and R. Mizuta, 2013: Changes in precipitation intensity over East Asia during the 20th and 21st centuries simulated by a global atmospheric model with a 60 km grid size. *J. Geophys. Res. Atmos.*, **118**, 11007−11016.

Mizuta, R., K. Oouchi, H. Yoshimura, A. Noda, K. Katayama, S. Yukimoto, M. Hosaka, S. Kusunoki, H. Kawai, and M. Nakagawa, 2006: 20-km-mesh global climate simulations using JMA-GSM model –Mean climate states–. *J. Meteor. Soc. Japan*, **84**, 165−185.

Mizuta, R., H. Yoshimura, H. Murakami, M. Matsueda, H. Endo, T. Ose, K. Kamiguchi, M. Hosaka, M. Sugi, S. Yukimoto, S. Kusunoki, and A. Kitoh, 2012: Climate simulations using MRI-AGCM3.2 with 20-km grid, *J. Meteor. Soc. Japan*, **90A**, 233−258.

Mizuta, R., O. Arakawa, T. Ose, S. Kusunoki, H. Endo, and A. Kitoh, 2014: Classification of CMIP5 future climate responses by the tropical sea surface temperature changes. *SOLA*, **10**, 167−171.

Mizuta, R., and co-authors, 2017: Over 5000 years of ensemble future climate simulations by 60km global and 20km regional atmospheric models. *Bull. Amer. Meteor. Soc.*, doi:10.1175/BAMS-D-16-0099.1.

Murakami, H., R. Mizuta, and E. Shindo, 2012a: Future changes in tropical cyclone activity projected by multi-physics and multi-SST ensemble experiments using the 60-km-mesh MRI-AGCM. *Climate Dyn.*, **39**, 2569−2584.

Murakami, H., Y. Wang, H. Yoshimura, R. Mizuta, M. Sugi, E. Shindo, Y. Adachi, S. Yukimoto, M. Hosaka, S. Kusunoki, T. Ose, and A. Kitoh, 2012b: Future changes in tropical cyclone activity projected by the new high-resolution MRI-AGCM. *J. Climate*, **25**, 3237−3260.

Ogata, T., R. Mizuta, Y. Adachi, H. Murakami, and T. Ose, 2016: Atmosphere-ocean coupling effect on intense tropical cyclone distribution and its future change with 60 km-AOGCM. *Scientific Reports*, **6**, doi:10.1038/srep29800.

Oouchi, K., J. Yoshimura, H. Yoshimura, R. Mizuta, S. Kusunoki, and A. Noda, 2006: Tropical cyclone climatology in a global warming climate as simulated in a 20 km-mesh global atmospheric model: Frequency and wind intensity analyses. *J. Meteor. Soc. Japan*, **84**, 259−276.

Roberts, M. J., P. L. Vidale, M. S. Mizielinski, M.-E. Demory, R. Schiemann, J. Strachan, K. Hodges, R. Bell, and J. Camp, 2015: Tropical cyclones in the UPSCALE ensemble of high-resolution global climate model. *J. Climate*, **28**, 574−596, doi:10.1175/JCLI-D-14-00131.1.

Rowell, D. P., C. K. Folland, K. Maskell, and M. N. Ward, 1995: Variability of summer rainfall over tropical North Africa (1906−92): Observations and modelling. *Quart. J. Roy. Meteor. Soc.*, **121**, 669−704.

Seo, K.-H., J. Ok, J.-H. Son, and D.-H. Cha, 2013: Assessing future changes in the East Asian summer monsoon using CMIP5 coupled models. *J. Climate*, **26**, 7662−7675.

Sugi, M., R. Kawamura, and N. Sato, 1997: A study of SST-forced variability and potential predictability of seasonal mean fields using the JMA global model. *J. Meteor. Soc. Japan*, **75**, 717−736.

Sugi, M., H. Murakami, and K. Yoshida, 2016: Projection of future changes in the frequency of intense tropical cyclones. *Climate Dyn.*, doi:10.1007/s00382-016-3361-7.

Wang, B., Q. Ding, X. Fu, I.-S. Kang, K. Jin, J. Shukla, and F. Doblas-Reyes, 2005: Fundamental challenge in simulation and prediction of summer monsoon rainfall. *Geophys. Res. Lett.*, **32**, L15711, doi:10.1029/2005GL022734.

Wehner, M. F., K. A. Reed, F. Li, Prabhat, J. Bacmeister, C.-T. Chen, C. Paciorek, P. J. Gleckler, K. R. Sperber, W. D. Collins, A. Gettelman, and C. Jablonowski, 2014: The effect of horizontal resolution on simulation quality in the Community Atmospheric Model, CAM5.1. *J. Adv. Model. Earth Syst.*, **6**, 980−997, doi:10.1002/2013MS000276.

Xie, S.-P., C. Deser, G. A. Vecchi, M. Collins, T. L. Delworth, A. Hall, E. Hawkins, N. C. Johnson, C. Cassou, A. Giannini, and M. Watanabe, 2015: Towards predictive understanding of regional climate change. *Nat. Clim. Change*, **5**, 921−930, doi:10.1038/nclimate2689.

Yoshimura, H., R. Mizuta, and H. Murakami, 2015: A spectral cumulus parameterization scheme interpolating between two convective updrafts with semi-Lagrangian calculation of transport by compensatory subsidence. *Mon. Wea. Rev.*, **143**, 597−621.

Manuscript received 31 August 2016, *accepted 3 December 2016*
SOLA: *https://www.jstage.jst.go.jp/browse/sola/*